International Journal of Fracture 101 (4) (2000) 321-345

The Separation of the Fracture Energy in Metallic Materials

Stampfl Jürgen* and Kolednik Otmar
(koledni k@unileoben.ac.at)
Erich Schmid Institut of Materials Science, Austrian Academy of Sciences, and Institute of Metal Physics, University of Leoben, Jahnstrasse 12, A-8700 Leoben, Austria

1998/02/11

Abstract. The total plastic strain energy which is consumed during fracture of a plain-sided CT specimen is separated into several components. These are the energies required for deforming the specimen until the point of fracture initiation, for forming the flat-fracture surfaces, for forming the shear-lip fracture surfaces, and for the lateral contraction and the blunting at the side-surfaces, W_{lat}. Characteristic crack growth resistance terms, R_{flat} and R_{slant}, are determined describing the energies dissipated in a unit area of flat-fracture and slant-fracture surface, respectively. R_{flat} is further subdivided into the term R_{surf}, to form the micro-ductile fracture surface, and into the subsurface term, R_{sub}, which produces the global crack opening angle.

Two different approaches are used to determine the fracture energy components. The first approach is a single-specimen technique for recording the total crack growth resistance (also called energy dissipation rate). Plain-sided and side-grooved specimens are tested. The second approach rests on the fact that the local plastic deformation energy can be evaluated from the shape of the fracture surfaces. A digital image analysis system is used to generate height models from stereophotograms of corresponding fracture surface regions on the two specimen halves.

Two materials are investigated: a solution annealed maraging steel V 720 and a nitrogen alloyed ferritic-austenitic duplex steel A 905. For the steel V 720 the following values are measured: $J_{\mathrm{i}} = 65\,\mathrm{kJ/m^2}$, $R_{\mathrm{surf}} = 20\,\mathrm{kJ/m^2}$, $R_{\mathrm{flat}} = 280\,\mathrm{kJ/m^2}$, $R_{\mathrm{slant}} = 1000\,\mathrm{kJ/m^2}$, $W_{\mathrm{lat}} = 30\,\mathrm{J}$. For the steel A 905 which has no shear lips, the measured values are: $J_{\mathrm{i}} = 190\,\mathrm{kJ/m^2}$, $R_{\mathrm{flat}} = 1000\,\mathrm{kJ/m^2}$, and $W_{\mathrm{lat}} = 45\,\mathrm{J}$. Apart from materials characterization, these values could be useful for predicting the influence of specimen geometry and size on the crack growth resistance curves.

Keywords: elastic-plastic fracture mechanics, fracture energy, energy dissipation rate, fracture surface analysis

Abbreviations: lsy – large-scale yielding; ssy – small-scale yielding; gy – general yielding; DEM – digital elevation model

1. Introduction

The crack growth resistance of a material depends on the total amount of non-reversible energy which is consumed during a fracture process. In fracture

* Current address: Rapid Prototyping Lab, Stanford University, Stanford CA 94305, USA

mechanics tests it is often observed that the crack growth resistance depends on the geometry and the size of the specimen (e.g., see [1] for an outline of the problem). This effect is noticed for a wide class of low-strength or medium-strength engineering materials where a large plastic zone accompanies the crack tip during crack propagation, i.e. for fracture under large-scale yielding (lsy) or general yielding (gy) conditions. Even if the consideration is confined to deeply notched bend-type specimen, the influence of geometry is significant.

As a consequence of these observations, two fundamental questions appear. The first question is: How can the crack growth resistance of these materials be characterized? The second question, in the literature referred to as "transferability problem", is: How can fracture toughness data, that are measured on a specific specimen, be transferred to specimens of other geometries or to a structural component of arbitrary shape? Both questions have yet to be resolved.

The geometry problem occurs because the local fracture properties of materials depend on the constraint. Different constraint measures have been introduced in the literature [2–6]. In the low-constraint near-side-surface regions of a deeply notched bend-type specimen the material behaves tougher then in the high-constraint mid-section region. Usually, this behavior is reflected in the fracture surface appearance: we see a flat-fracture mid-section region accompanied by two shear lip regions with slant fracture surfaces near the side surfaces. The global fracture properties of the material result as a complicated interplay of all the different constraint conditions along the crack front [7].

A promising way to resolve the geometry problem would be to separate the total plastically deformed region into several characteristic parts and to predict the amount of the plastic strain energy dissipated in each part. By doing this, we can extract a value of the crack growth resistance for the high-constraint region, that might be characteristic for the material. (Another characteristic value, for the low-constraint region directly near the side-surface, might exist, too.) This would answer the first question posed, and it would be also an important step towards solving the transferability problem.

For a separation to be successful, it is not only necessary that it is clearly defined and conceptually feasible; it is also strongly desired that the amount of plastic strain energy consumed in each part can be determined experimentally. Existing theories about the geometry influence on the crack growth resistance, [1–3, 5, 6, 8–10], could not be proved and new, improved theories could not be derived, otherwise. To the knowledge of the authors no such separation has been reported so far.(A short literature survey will be given below.)

We will demonstrate in this study that it is possible to separate the total plastic strain energy for the fracture of Compact Tension specimens made

of two different steels in a reasonable way and to measure all the energy components. The general outline of the procedure is shown in Fig. 1. Two different approaches are used. The first approach is an indirect one: different fracture mechanics experiments are designed so that a careful analysis allows the separation of the total fracture energy into several characteristic parts. The second approach is a more direct one: the local plastic deformation energy is estimated from the topography of the fracture surfaces. Plastic deformation during fracture produces a misfit between corresponding fracture surface regions on both parts of the broken specimen, which can be analyzed to determine the locally dissipated plastic strain energy.

The combination of both approaches could be a powerful means towards a solution of the geometry problem.

2. A Brief Literature Survey

2.1. THE DEFINITION OF THE TOTAL CRACK GROWTH RESISTANCE

The total crack growth resistance, R_{tot}, of a material can be defined as total non-reversible energy which is necessary to extend the crack area by an increment, see Turner and Kolednik [11],

$$R_{\mathrm{tot}} \equiv \frac{1}{B}\frac{d}{d(\Delta a)}\left(W_{\mathrm{pl,tot}} + \Gamma\right). \tag{1}$$

$W_{\mathrm{pl,tot}}$ denotes the total non-reversible strain energy consumed during the fracture process, Γ is the surface energy, Δa the crack extension and B the specimen thickness. For elastic ideally brittle materials, $W_{\mathrm{pl,tot}} = 0$ and R_{tot} reduces to the Griffith solution [12], i.e. to twice the specific surface energy, $R_{\mathrm{tot,el}} = 2\gamma_0$. If plasticity were confined to a constant, narrow zone around the crack tip , the Orowan [13] and Irwin [14] approach of the existence of a specific non-linear fracture surface energy would be applicable: $R_{\mathrm{tot,sssy}} = 2(\gamma_0 + \gamma_{\mathrm{pl}}) = const.$ The subscript "sssy" indicates that the confinement of the plastic zone must be even stronger than for small-scale yielding (ssy) conditions. For most elastic-plastic materials even for sssy-conditions the specific plastic strain energy for fracture exceeds the specific surface energy by several orders of magnitude, $\gamma_{\mathrm{pl}} \gg \gamma_0$. It should be remarked that for micro-crack toughening, fiber reinforced, or transformation toughened materials with brittle matrices additional non-reversible energy terms appear, originating from processes other than plastic deformation, [15–17]. These energy terms must be included on the right-hand side of Eq. (1).

The total crack growth resistance, R_{tot}, was introduced by Turner [1]. He called R_{tot} the "energy dissipation rate", symbolized by the letter D. This

nomenclature might be somewhat misleading, because parts of the energies in Eq. (1) are not really dissipated during fracture [11]. Apart from the terms just mentioned above, these are the non-reversible elastic strain energy that originates due to the non-homogeneous crack-tip field, [18], and the surface energy.

Since some confusion seems to exist in the literature, a note regarding the reversibility of fracture energies is presented in Appendix A. An important analysis on the thermodynamics of fracture was published by Gurney [19].

2.2. SOME PREVIOUS IDEAS ON THE SEPARATION OF FRACTURE ENERGIES

The idea of the separation of the fracture energies is not new. Cotterell and Reddel [20] performed fracture tests on thin double-edged notched panels with different ligament lengths. The total work of fracture was measured for each test and plotted against the ligament length. This diagram displayed a linear relationship. By extrapolating the linear regression line to zero ligament length, an "essential work of plane stress fracture" was determined, which depended on the specimen thickness. It was claimed that the essential work of fracture corresponds to the work done in the crack-tip region, distinct from the work done in the outer plastic regions. Based on the same idea, several other studies were performed later, e.g. [21, 22].

Turner [1], and John and Turner [23] discovered that resistance curves in terms of the total crack growth resistance, i.e. R_{tot}-Δa-curves, show typically a regime of steady-state growth after a short transition region of decreasing R_{tot}. They compared the curves for side-grooved and plain-sided specimens and attempted to break the steady-state value, $R_{\mathrm{tot,ss}}$, into two [1] or three [9] components to find characteristic terms of dissipated energy per unit of crack area, or per unit of (shear-lip) volume. These terms, called "specific intensities of the rate of energy dissipation" (SIRED), were then used to predict the resistance curves for other (bend-type) geometries. However the procedure has not been completely successful so far. One possible limitation was that only a multi-specimen method had been used to record the R_{tot}-Δa-curves, compared to the single-specimen technique applied in this investigation.

Another interesting approach was chosen by Shoji [24]: he sliced bend and CT specimens made of a bainitic steel perpendicular to the crack plane and measured the plastic strains near the fracture surfaces by applying a recrystallization-etch technique. The local plastic strain values were used to evaluate for the mid-section region the plastic strain energy within an intensely deformed region around the crack tip. This value was found to be independent of crack extension. A similar experiment, with specimens of different thicknesses, was conducted in [25].

Stüwe [26, 27] developed a model to estimate the specific plastic strain energy to form a micro-ductile fracture surface from the dimple height (see Fig.2). A short description of the model will be given in Section 6.2. In [28] the fracture surface energy was determined for a maraging steel, similar to the one used in the current study. The dimple height was measured by stereo-photogrammetric analyses of corresponding fracture surface regions on both specimen halves [29, 33].

Mecklenburg et al. [30] determined for three steels the rates of the elastic, the plastic, and the total strain energies versus the crack extension for side-grooved CT specimens. They observed that after a short crack extension a steady-state condition was reached. The sizes of the energy rates depended on the initial crack length and the specimen size.

3. The Total Plastic Strain Energy for Fracture and its Components

3.1. The different plastic strain energy terms

In a micro-ductile plane-strain fracture experiment (e.g., using a specimen with side grooves) plastic strain energy, $W_{\mathrm{pl,surf}}$, is consumed to form the dimple structure of the fracture surfaces. This term is connected to the void growth and coalescence processes occurring within the process zone directly in front of the crack tip. For sssy-conditions, $R_{\mathrm{surf}} = W_{\mathrm{pl,surf}}/(B\Delta a)$ will come close to the size of $R_{\mathrm{tot,sssy}}$. In all other cases additional energy, $W_{\mathrm{pl,sub}}$, is necessary for the deformation below the fracture surfaces. The sum of both, surface plus subsurface term, is the plastic energy for flat fracture, $W_{\mathrm{pl,flat}}$.

To fracture a smooth-sided specimen (without side grooves) $W_{\mathrm{pl,flat}}$ is needed for the flat fracture regions in the center of the specimen. $W_{\mathrm{pl,slant}}$ shall denote the energy (surface plus subsurface) for producing the slant fracture of the shear lip regions near the side surfaces. Additional plastic energy is needed for the lateral contraction of the side surfaces and for the blunting process at the side surfaces, both combined in the term $W_{\mathrm{pl,lat}}$. Another term, $W_{\mathrm{pl,i}}$, is necessary for fracture initiation, i.e. for deforming the material until to the point when the first crack extension occurs in the specimen center. The total plastic strain energy (consumed until a certain amount of total crack extension or until final fracture), $W_{\mathrm{pl,tot}}$, is given by

$$W_{\mathrm{pl,tot}} = W_{\mathrm{pl,i}} + W_{\mathrm{pl,flat}} + W_{\mathrm{pl,slant}} + W_{\mathrm{pl,lat}}. \qquad (2)$$

It should be noted that both the second and the third term of Eq.(2) might contain also some remote plasticity appearing near the back face of the specimen.

Since $W_{\mathrm{pl,i}}$ remains unchanged after fracture initiation, it does not influence the size of R_{tot}. Thus, the totally consumed non-reversible energy during fracture can be written as

$$W_{\mathrm{pl,tot}} = W_{\mathrm{pl,i}} + \int_0^{\Delta a} R_{\mathrm{tot}}\, d(\Delta a). \tag{3}$$

3.2. A GENERAL OUTLINE FOR DETERMINING THE ENERGY TERMS

The indirect approach to determine the different energy terms relies on the measurement of the crack growth resistance of the materials not only in terms of the commonly used J-integral vs. crack extension ($J - \Delta a$-) curves, but also in terms of the total crack growth resistance, R_{tot}, vs. Δa curves.

$W_{\mathrm{pl,i}}$ is evaluated from the area under the load vs. load-line displacement curve at the point of fracture initiation (which is detected by a potential drop technique). $W_{\mathrm{pl,flat}}$ and the fracture properties of the specimen center region are derived from a test of a side-grooved specimen (see Fig. 1). $W_{\mathrm{pl,slant}}$ is determined from the resistance curve of a thin specimen where the two shear lip regions merge into one slant fracture surface. $W_{\mathrm{pl,lat}}$ can be measured as the shaded area in the $R_{\mathrm{tot}} - \Delta a$-curves in Fig. 1. This is deduced from the results of a multi-specimen test and demonstrated on specimens with different thicknesses.

In a previous investigation a digital image analysis procedure for reconstructing the topography of fracture surfaces from stereo photograms taken in the scanning electron microscope was developed [31, 32]. This technique is used for the direct approach to determine the fracture energy terms. From the topographic measurements the fracture surface energy, $W_{\mathrm{pl,surf}}$, is evaluated using Stüwe's model. The new technique allows the automatic analysis of whole fracture surface regions, compared to the time consuming point-per-point analysis which had to be done in [28, 29, 33]. This enables $W_{\mathrm{pl,surf}}$ to be estimated much faster and more accurately than in previous work [34, 35].

Our new technique for analyzing fracture surfaces can be also applied to measure the crack opening angle, COA, near the mid-section of the specimens. This allows the determination of $W_{\mathrm{pl,sub}}$ for the flat-fracture region.

4. Materials and Specimens

The separation of the total fracture energy is demonstrated on two materials. The first material is a solution annealed maraging steel V 720. The steel was forged, solution annealed for 1 hour at 820°C, and subsequently cooled in air. The tensile tests resulted a yield strength of $\sigma_{\mathrm{y}} = 750$ MPa, an ultimate tensile strength of $\sigma_{\mathrm{u}} = 1050$ MPa and a strain hardening exponent of $n =$

0.15. The Young's modulus is $E = 193$ GPa. The chemical composition is given in Tab. I.

The second material is a nitrogen alloyed ferritic-austenitic duplex steel A 905. After the forging the steel was solution annealed for 30 minutes at 1100°C and water quenched. Due to this treatment the steel has a microstructure of elongated domains of about 50% austenite and ferrite. The tensile properties (perpendicular to the crack plane) are $\sigma_{\rm y} = 630$ MPa, $\sigma_{\rm u} = 950$ MPa, $n = 0.20$ and $E = 215$ GPa. The chemical composition is given in Tab. II.

From both materials Compact Tension (CT-) specimens were machined in a S-T-crack plane orientation, i.e. the elongated domains of the steel A 905 lie parallel to the crack front. The specimens had a width of $W = 50$ mm, an initial crack length $a_0 \approx 28$ mm and a thickness of $B = 25$ mm. For the steel V 720 thinner specimens were tested, too.

5. An Indirect Procedure to Separate Fracture Energies

In this section characteristic plastic energy terms are extracted from fracture mechanics tests conducted with side-grooved specimens and plain-sided specimens of different thicknesses. J-integral versus crack extension (J-Δa) curves were recorded following the ESIS [36] and ASTM [37] Standard Procedures. The $R_{\rm tot}$-Δa -curves were determined by a single-specimen technique which is described in the following section.

5.1. SINGLE SPECIMEN TESTS

5.1.1. *A single specimen technique for measuring the total crack growth resistance*

Eq. (1) can be extended by considering the balance of energy during an increment of crack extension [11],

$$R_{\rm tot} \equiv \frac{1}{B}\frac{d(W_{\rm pl}+\Gamma)}{d(\Delta a)} = \frac{1}{B}\frac{d(U-W_{\rm el})}{d(\Delta a)} \equiv C. \tag{4}$$

The right-hand side extension of Eq. (4) can be seen as the crack driving force, C which balances $R_{\rm tot}$ during equilibrium crack growth. It is used to evaluate $R_{\rm tot}$ experimentally. U is the external energy which can be measured by integrating the area below the load vs. load-line displacement (F-$v_{\rm LL}$-) curve. The reversible elastic strain energy, $W_{\rm el}$, can be determined by measuring the load, F, and applying the relation

$$W_{\rm el} = \frac{\phi F^2}{2}, \tag{5}$$

where ϕ denotes the compliance of the specimen. For the side-grooved specimen ϕ is evaluated for an effective thickness, B_{e}. Formulae for ϕ and B_{e} are given in the Standard Procedures [36, 37].

If the current crack length is known, R_{tot} can be evaluated by differentiating numerically the $(U - W_{\mathrm{el}})$ vs. Δa-curve. The current crack length is determined by the direct-current potential drop technique.

5.1.2. *Test results of the plain sided specimens*

On the left-hand side of Fig. 3 the R_{tot}-Δa-curves of the plain sided specimens are plotted, together with the conventional J-integral vs. crack extension (J-Δa-) curves. Both R_{tot}- Δa-curves exhibit sharp peaks at or near the point of fracture initiation. For the steel A 905, R_{tot} falls down after the peak to a lower plateau value of $R_{\mathrm{tot}} \approx 2000\,\mathrm{kJ/m^2}$. Between $\Delta a = 1.7$ and 2.8 mm a second peak can be observed with a maximum value of $\hat{R}_{\mathrm{tot}} \approx 4000\,\mathrm{kJ/m^2}$ at $\widehat{\Delta a} = 2.5$mm. For the steel V 720 the picture is not so clear. It is possible to detect a lower plateau value of about $R_{\mathrm{tot}} \approx 270$ kJ/m^2 combined with a very broad peak between $\Delta a = 2.5$ to 11 mm. The second R_{tot}-peak, $\hat{R}_{\mathrm{tot}} \approx 800$ kJ/m^2, lies at $\widehat{\Delta a} = 6.2$ mm. The J-Δa-curves yield fracture initiation values of $J_{\mathrm{i}} = 65$ kJ/m^2 for the steel V 720 and $J_{\mathrm{i}} = 200$ kJ/m^2 for the steel A 905.

Beyond the initial part, the R_{tot}-Δa-curves look like the first derivatives of the J-Δa-curves. This is reasonable because for general-yielding conditions R_{tot} and the slope of the J-Δa -curve are directly related (and not R_{tot} and J!) [38]. For deeply notched bend-type specimens the relation reads (see Appendix B)

$$\frac{dJ}{d(\Delta a)} \approx \frac{\eta}{b} R_{\mathrm{tot}}. \tag{6}$$

b is the ligament length, $b = W - a$, and η is the pre-factor in the formula to evaluate J from the area, U, below the F-v_{LL}-curve,

$$J = \frac{\eta U}{bB}. \tag{7}$$

In [8] a relation between the slope of the J-Δa-curve and R_{tot} was deduced that is valid for ssy-conditions as well. As was pointed out by Kolednik [8, 38], the significance of Eq. (6) lies in the fact that it clearly demonstrates that for elastic-plastic materials the J-Δa-curve does not scale to the crack growth resistance. This fact was noticed later by Atkins [39], and Cotterell and Atkins [40], too.

The first peak of the R_{tot}-Δa-curve is a result of crack tip blunting. It was found in [42] that the point of fracture initiation in the center region is correlated to the (first) inflection point of the R_{tot}-Δa-curve. To understand the significance of the second peak we conducted an extensive multi-specimen

test on the steel V 720. Before discussing this multi-specimen test, the testing results of the side-grooved specimens shall be presented.

5.1.3. *Test results of the side-grooved specimens*
We performed these single-specimen tests with 20% side grooved specimens, $B_{\rm n} = 20\,$mm. The results are shown on the right-hand side of Fig. 3.

The $R_{\rm tot}$-Δa-curve of the steel V 720 shows a sharp peak at initiation followed by a very short plateau region with $R_{\rm tot} \approx 280$ kJ/m^2 (which comes close to the lower plateau value of the non-sidegrooved specimen seen in Fig. 3). We doubt that the decrease of $R_{\rm tot}$ after $\Delta a \approx 0.6$ mm is significant because the crack growth became unstable afterwards. The decrease in $R_{\rm tot}$ is caused probably by the increase of the crack velocity. Thus, we take $R_{\rm flat} \approx 280$ kJ/m^2 as the approximate value of the crack growth resistance for the (steady-state) flat-fracture region, although there remains some uncertainty for larger Δa-values. The J -Δa-curve shows a fracture initiation value that is similar to that for the non-side grooved specimen, $J_{\rm i} = 70\,$kJ/m^2.

A similar behavior was observed for the steel A 905. After the initiation peak, the $R_{\rm tot}$-Δa-curve slowly decreases to a value of about $R_{\rm tot} \approx 1000$ kJ/m^2. This value is taken as approximating $R_{\rm flat}$. Due to the increased crack velocity the few data points measured beyond $\Delta a \approx 1.4$ mm are questionable. From the J-Δa-curve we get $J_{\rm i} = 190\,$kJ/m^2.

It should be stated that side-grooved specimens do not necessarily give $R_{\rm flat}$-values. In very tough materials some lateral contraction can be observed in spite of the side-grooves.

5.2. A MULTI-SPECIMEN TEST ON THE STEEL V-720

In Fig. 6 the heat-tinted surfaces of the 12 broken specimens of the steel V 720 are shown. It can be seen that the crack extension in the center region of the specimen is about $15\,$mm when the crack begins to grow near the side surfaces. In Fig. 4 the local crack extensions in the mid-section, $\Delta a_{\rm M}$, and at the side surfaces, $\Delta a_{\rm S}$, are plotted with respect to the load-line displacement.

Near the mid-section the crack growth is initiated at $v_{\rm LL} \approx 0.5$ mm. At a load-line displacement of about $v_{\rm LL} \approx 2$ mm crack growth starts at the side surfaces. At the same moment the crack growth rate in the center region slows down appreciably because the crack already approaches the neutral axis of the CT-specimen. From the $v_{\rm LL}$-Δa-curve (which is not included here) it is seen that at $v_{\rm LL} = 2\,$mm the crack extension amounts $\Delta a \approx 6.3\,$mm. At this value the $R_{\rm tot} - \Delta a$ curve has its second peak. Thus, it is concluded that this peak appears at (or shortly before) the moment where crack growth is initiated at the side surfaces. A similar observation was made in [41] for another material.

It is interesting to check the lateral contraction of the plain-sided specimens. The maximum deformation in thickness (z-) direction (which amounts 0.32 mm on each side) is reached when the crack extension starts near the side surfaces. During further crack extension at the side surfaces a "lateral contraction zone" moves with the crack front, but the amount of additional z-deformation decreases.

The results of this section suggest that the second peak of the R_{tot}- Δa-curve may originate from the blunting process near the side-surface regions and the lateral contraction of the specimen. The curve displays its second maximum at the point of initiation of crack growth near the side surfaces.

To prove this hypothesis R_{tot}-Δa-curves were analyzed for specimens with different thicknesses.

5.3. THE INFLUENCE OF SPECIMEN THICKNESS

From the steel V 720 additional single specimen tests were conducted on specimens having thicknesses of $B = 16$, 8, and 4 mm. The resulting R_{tot}-Δa- and J-Δa-curves are collected in Fig. 5.

All J-integral initiation values lie about $J_{\mathrm{i}} = (60 - 65)$ kJ/m^2. It is noteworthy that with decreasing thickness the second peak of the R_{tot}-Δa-curve is shifted to lower Δa-values: $\widehat{\Delta a} = 6.2$, 4.5, 1.8 and 1.1 mm for $B = 25, 16, 8$ and 4 mm. The height of the second peak increases: $\widehat{R_{\mathrm{tot}}} = 800$, 1100, 3700 and 5800 kJ/m^2.

Of particular interest is the R_{tot}-Δa-curve of the thinnest specimen, $B = 4$ mm, where the first and second peak merge into one peak. After a mean crack extension of $\Delta a \approx 2.3$ mm a steady-state condition seems to be reached when $R_{\mathrm{tot}} = 1000$ kJ/m ^{2}. The fracture surface reveals a short, cuspated flat fracture region. The two shear lip regions join and form one slant fracture surface region.

The lateral contraction of the specimens was studied, too. In each specimen the z-deformation is largest at the position of the stretched zone in the mid-section of the specimen. By comparing different specimens it can be observed that the z-deformation reaches its maximum value at that point when crack growth is initiated at the side surfaces. The lateral contraction process is about to be completed when the end of the second peak of the R_{tot}- Δa-curve is reached, e.g. at $\Delta a \approx 2.3$ mm for the thinnest specimen. The mean crack extension where the lateral contraction process is completed, will depend on the ligament length. For a specimen with a very large ligament length, e.g., a Double Cantilever Beam (DCB) specimen, or ideally, an infinite clamped strip, the lateral contraction process would not cease and a steady-state contraction zone would move with the crack front.

This point leads to the conclusion that the steady-state R_{tot} of this specimen after the peak characterizes the crack growth resistance for producing

a slant shear-lip fracture surface. Thus, we get for the steel V 720 a characteristic value of $R_{\mathrm{slant}} = 1000$ kJ/m^2. The ratio $R_{\mathrm{slant}}/R_{\mathrm{flat}}$ has a size of 3.6.

5.4. Fracture surface analysis on the steel A 905

Fig. 7 presents the fracture surface of a plain sided specimen made of the steel A 905. No shear lips can be found. The reason is that the ferritic domains in front of the crack tip fail at low loads by cleavage or quasi-cleavage fracture [42]. At these low loads the width of the low-constraint side-surface region, which scales with the plastic zone size, is small and, as a consequence, no shear lips can be formed. A similar observation was made on a mild steel containing long MnS-inclusions [29]: the critical plastic strain for void nucleation is very small, hence no shear lips can be formed.

A section parallel to the crack front shows that the flat fracture surfaces bend concavely near the side surfaces. It seems as if the crack growth resistance for flat fracture, R_{flat}, increases gradually when approaching the side surfaces due to an increase of the subsurface energy, $W_{\mathrm{pl,sub}}$. The two regions of enhanced R_{flat} are 6 to 7 mm broad (observe the development of the stretched zone width along the crack front in Fig. 7).

The lateral contraction of this specimen is quite large, too. The maximum z-deformation amounts 1.16 mm on each side.

Summarizing this section, it is stated that there exists no unique characteristic value of the crack growth resistance of the near-side surface regions for the steel A 905.

5.5. The separation of the fracture energies

5.5.1. *General remarks*

As a basic hypothesis for the separation of the total plastic strain energy, $W_{\mathrm{pl,tot}}$, into its components (via the indirect approach) it is assumed that there exist characteristic values of the crack growth resistance to form either the (plane strain) flat-fracture surfaces, R_{flat}, or the slant shear lip surfaces, R_{slant}. R_{flat} and R_{slant} should be independent of crack extension and specimen thickness. This assumption does not seem unrealistic, as long as we consider deeply notched CT- or bend type specimen.

The separation is demonstrated on five specimens of the steel V 720 (plain sided specimens with thicknesses $B = 25$, 16, 8, 4 mm and side grooved specimen) and on the two specimens of the steel A 905. All the results of the separation procedure are collected in Table III.

The fracture surfaces of each (heat tinted) specimen were photographed in the scanning electron microscope. On each photo the final average crack extension, Δa_{tot}, was measured. The boundary between the flat-fracture and

the slant-fracture region was marked. and the sizes of the corresponding fracture surface areas, $\Delta A_{\rm flat}$ and $\Delta A_{\rm slant}$, were determined. The plastic strain energies to form either the flat or the slant fracture surfaces are estimated by

$$W_{\rm pl,flat} = R_{\rm flat}\,\Delta A_{\rm flat} \tag{8}$$

or

$$W_{\rm pl,slant} = R_{\rm slant}\,\Delta A_{\rm slant}. \tag{9}$$

The values $R_{\rm flat} = 280\,{\rm kJ/m^2}$ and $R_{\rm slant} = 1000\,{\rm kJ/m^2}$ were used for the steel V 720, and $R_{\rm flat} = 1000$ kJ/m^2 for the steel A 905. For the latter material $W_{\rm pl,slant}$ was not determined because no shear lips were observed.

The second peak of the $R_{\rm tot}$-Δa-curve was ascribed to the blunting process near the side-surface regions and to the lateral contraction of the specimen. Accordingly, the plastic strain energy term $W_{\rm pl,lat}$ can be evaluated by integrating numerically the area under the second peak in the $R_{\rm tot}$-Δa-curve. (The area is taken above an estimated "baseline" that is given, e.g. for the steel A 905 by the steady-state value $R_{\rm tot} = 2000\,{\rm kJ/m^2}$.)

The $W_{\rm pl,i}$- and the $W_{\rm pl,tot}$-values are taken from the areas, U, under the load vs. load-line displacement curves by subtracting the elastic energy, Eq.(5).

5.5.2. *Discussion of the results*

Table III lists the following data: the final crack extension, $\Delta a_{\rm tot}$; the J-integral at fracture initiation in the center, $J_{\rm i}$;the flat-fracture area, $\Delta A_{\rm flat}$, and the slant-fracture area, $\Delta A_{\rm slant}$; the plastic strain energies for fracture initiation in the center, $W_{\rm pl,i}$, for forming the flat-fracture area, $W_{\rm pl,flat}$, for forming the slant-fracture area, $W_{\rm pl,slant}$, and for side-surface blunting and lateral contraction, $W_{\rm pl,lat}$; the sum of the estimated plastic fracture energies, $\sum W_{\rm pl,est} = W_{\rm pl,i} + W_{\rm pl,flat} + W_{\rm pl,slant} + W_{\rm pl,lat}$, and the total plastic strain energy, $W_{\rm pl,tot}$, measured in the tests.

It is interesting to note that $W_{\rm pl,lat} \approx 30$ J for the three thickest plain sided specimens of the steel V 720. This suggests that the plastic strain energy for side-surface blunting and lateral contraction is constant as long as the specimen is thick enough, so that the two shear lip regions are still separated by a flat-fracture region.

The ratio $W_{\rm pl,lat}/W_{\rm pl,tot}$ gives the percentage of the total non-reversible fracture energy that comes from blunting and lateral contraction at the side surfaces. This ratio is remarkably large: For the steel V 720 the values are (with decreasing thickness) 26, 43, 69 and 61%, and for the steel A 905 it is 22%. (It should be kept in mind that the final crack extension of the specimens differs. All specimens were loaded at least up to the end of the second peak of the $R_{\rm tot}$-Δa-curve. The reason for the different $\Delta a_{\rm tot}$-values is that thinner specimens exhibit larger load-line displacement values and the tests had to be stopped before the clip gauge went out of range.)

A principle error is made in connection with the term $W_{\mathrm{pl,i}}$. The reason is that at the point of fracture initiation, $J = J_{\mathrm{i}}$, the crack extension has already reached a small, but finite value, Δa_{i}. ΔA_{i} denotes the flat-fracture surface area at initiation. Thus, some plastic strain energy to produce ΔA_{i} is counted twice, because it is included in both the $W_{\mathrm{pl,i}}$, as well as in the $W_{\mathrm{pl,flat}}$ term. However, this error will be negligeable in most cases except for small Δa_{tot}-values.

The sum of the estimated plastic fracture energies coincides quite well with the measured total plastic strain energy. The only exception is the plain sided specimen of the steel A 905, where the assumption of a constant R_{flat} is clearly not met, see Section 5.4.

Although no firm proof, this strongly suggests that our assumption of characteristic values of R_{flat} (for both steels) and R_{slant} (for the steel V 720) is correct. No data are available of specimens with other ligament lengths or other sizes. As far as it concerns highly constraint bend-type specimens, we expect that the characteristic values would be the same. However, we do not know how the flat-fracture and shear-lip fracture values would change for specimens with a low global constraint, like center-cracked tensile specimens. Whether the plastic strain energy for side-surface blunting and lateral contraction, $W_{\mathrm{pl,lat}}$ can be treated as a characteristic value, remains unclear.

6. The Estimate of Fracture Energies from Fracture Surface Analyses

This section deals with the direct determination of characteristic plastic strain energies via stereophotogrammetric analyses of the fracture surfaces.

6.1. STEREOPHOTOGRAMMETRY

Stereophotogrammetric means have been applied for a long time in fracture research, e.g., to study the topography of fatigue crack surfaces [43], and of micro-ductile [29, 33, 44, 45] or cleavage [29, 46, 47] fracture surfaces. The first semi-automatic analyses were reported in [48, 49].

Recently, an already existing digital photogrammetry system [50] was used to develope an automatic system for fracture surface analysis. The topography of a fracture surface is reconstructed by taking stereophotograms in the scanning electron microscope (SEM) and analyzing the images with a system for automatic image processing. This system finds homologous points on the stereophotograms and generates a three-dimensional model of the fracture surface consisting of about 10.000 to 20.000 points. The model is called "digital elevation model", DEM. The computing time for an analysis is about ten minutes on a PC. The new system for automatic fracture surface analysis is described in more detail in [31, 32, 35].

6.2. THE PLANE STRAIN FRACTURE SURFACE ENERGY

In [26,27], Stüwe introduced a model to estimate the plastic strain energy that is necessary to form a ductile fracture surface, $W_{\mathrm{pl,surf}}$. A schematic cross-section of the broken specimen shows a series of dimples of height h_0, see Fig. 2. $W_{\mathrm{pl,surf}}$ is given by

$$W_{\mathrm{pl,surf}} = 2\int_0^{h_0} A(h)\left(\int_0^{\varphi(h)} \sigma(\varphi)d\varphi\right)dh \tag{10}$$

In Eq. (10) $A(h)$ denotes the cross section at height h, A_0 is the original cross section, φ is the logarithmic (plastic) strain and $\sigma(\varphi)$ is the flow stress. After inserting the relation $\varphi(h) = \ln\left(\frac{A_0}{A(h)}\right)$ and after division by A_0 the equation transforms to

$$R_{\mathrm{surf}} = \frac{W_{\mathrm{pl,surf}}}{A_0} = 2\overline{\sigma}\int_0^{h_0} \frac{A(h)}{A_0}\ln\left(\frac{A_0}{A(h)}\right)dh. \tag{11}$$

R_{surf} is the specific plastic strain energy to form the micro-ductile fracture surface profile depicted in Fig. 2. The surface energy term is neglected.

$\overline{\sigma}$ designates an appropriate mean flow stress of the material which can be estimated by [27]

$$\overline{\sigma} = \sigma_{\mathrm{u}}\frac{\exp(n)}{(1+n)n^n}, \tag{12}$$

using the approximation $\sigma = \sigma_0\varphi^n$ for the stress-strain curve where n is the strain hardening exponent and σ_0 a reference stress. Eq.(11) can be evaluated if the distribution of $A(h)$ versus h of the considered fracture surface regions is known.

It should be stated that the so determined value of $W_{\mathrm{pl,surf}}$, sums the plastic strain energies of the fracture surfaces from the point of void initiation until to final failure of the bridges between the voids. Some plastic deformation energy, $W_{\mathrm{pl,sub}}$, is additionally needed to initiate the voids. That means that, e.g. in the Irwin-Orowan case the total crack growth resistance must be somewhat larger, $R_{\mathrm{tot,sssy}} \geq R_{\mathrm{surf}}$, although the difference might be very small.

The knowledge of the topography of one fracture surface is not sufficient to evaluate Eq.(11), because the topography of one DEM could be compensated by the topography of its opposite from the second specimen half. For example, an ideally brittle material may exhibit a rough fracture surface, i.e. a certain distribution of $A(h)$ versus h on one specimen half, but the two broken pieces could be glued together without any misfit and R_{surf} would be zero. R_{surf} is determined by the misfit between the broken parts. That means

that the corresponding fracture surface regions on both parts of a broken specimen must be analyzed. The two opposite DEMs are then used to generate a void map [34] that contains the information about the misfit between the two fracture surfaces, i.e. the distribution of $A(h)$ versus h. with this Eq.(11) can be solved numerically.

The specific plane strain fracture surface energy, $R_{\rm surf}$, was determined on the steel V 720, only. (The austenitic-ferritic duplex steel A 905 shows a patchwork of micro-ductile and cleavage fracture surface regions. The determination of $R_{\rm surf}$ needs, therefore, a more sophisticated analysis, e.g. see [51], which has not been undertaken so far.) SEM-micrographs of two corresponding fracture surface regions near the stretched zone, together with the DEMs and crack profiles perpendicular to the crack front are presented in Fig. 8, 9 and 10. A void map can be found in [32].Table IV lists the estimated $R_{\rm surf}$-values. All four values lie around $R_{\rm surf} = 20\,{\rm kJ/m^2}$. It is interesting to note that even the same size is measured for the side-grooved specimen at a distance of 3 mm in front of the fatigue crack, which is well beyond the point where fracture became unstable.

6.3. THE DIRECT DETERMINATION OF $R_{\rm flat}$

From the preceding section it is seen that for the steel V 720 even in the flat-fracture region only 7% of the plastic energy is used to form the fracture surfaces. The remaining 93% are spent below the surface. This energy, $R_{\rm sub} = R_{\rm flat} - R_{\rm surf} = 260\,{\rm kJ/m^2}$, is needed to produce the global crack opening angle, COA, in the wake of the crack.

COA and $R_{\rm tot}$ are related by (see Appendix B)

$$COA = \frac{dCOD}{d\Delta a} \approx \frac{\eta}{m\sigma_{\rm y} b} R_{\rm tot}. \tag{13}$$

Eq.(13) considers the behavior of the total specimen: Δa is the average of the crack extension values along the crack front and $R_{\rm tot}$ is the total crack growth resistance. COA and COD can be imagined as global values similar to that determined from the load-line displacement by adopting a plastic-hinge opening model with a fixed rotational center. However, Eq.(13) can be applied for a local description, too: COD and Δa are then local values measured at a given position along the crack front, and COA is, thus, a measure of the local crack growth resistance. To describe the behavior of the flat-fracture region Eq.(13) must be re-written as

$$COA_{\rm flat} = \frac{dCOD_{\rm flat}}{d\Delta a_{\rm M}} \approx \frac{\eta}{m\sigma_{\rm y} b} R_{\rm sub}. \tag{14}$$

Δa_{M} is the local crack extension in the mid-section. Inserting the data for the steel V 720 (with $m = 1.9$ from Eq.(18)), the COA-estimate results $COA_{\mathrm{flat}} = 1.0°$.

A series of low-magnification stereophotograms were taken from the mid-section region of specimen to determine COA_{flat} experimentally. Again, both specimen halves were analyzed. From the DEMs crack profiles were extracted, from which COD-Δa-curves and the crack opening angle could be measured. The measurement gave $COA_{\mathrm{flat}} = (1.4 \pm 0.3)°$. This is in reasonable agreement to the estimated value, especially when bearing in mind that the local COD-Δa-curve is bent and that only a 3 mm long region was analyzed. The curvature decreases with increasing Δa. This is because the local $CTOD$ at the current tip displays a transition regime of declining values before it reaches its steady-state value [1, 23, 55].

From the preceding paragraph it is learned that COA should be determined in the flat-fracture region at a distance of at least $2 - 3$ mm from the fatigue crack to compute R_{sub} from Eq.(14). The total value of R_{flat} is got by adding R_{sub} and R_{surf}. For tough materials the error, which is made by neglecting the surface term, will be in the order of a few percent, only.

6.4. The determination of the local fracture toughness

The new technique for fracture surface analysis is a perfect tool for determining the local fracture properties of a material. The local fracture initiation toughness can be measured in terms of the critical crack tip opening displacement, COD_{i}, and the local crack growth toughness can be measured in terms of the crack opening angle, COA. Both COD_{i} and COA increase near the side-surface. For example, in [29, 52] the scatter and the variation of COD_{i} along the crack front of a mild steel was studied. In [53] for the same steel the mid-section and side-surface COA-values were determined [1]. Surface and mid-section COA-measurements on aluminum alloys are reported in [54]. Additional stereophotogrammetric studies for the two steels V 720 and A 905 are being undertaken presently.

To characterize the fracture properties of materials the characteristic COD_{i}- and COA-values for the flat-fracture and the slant-fracture regions can be sought, and for solving the transferability problem the variation of these values along the crack front (and with crack extension) can be analyzed. With

[1] These COA-values were transformed in [53] to $CTOA$-values taken 0.1 mm behind the current crack tip. The two $CTOA$-values (for the mid-section and the side-surface) were used subsequently to control the crack extension in the numerical analysis. In both the experimental determination and the application for controlling the crack growth in numerical studies, it is important to distinguish between global COA and local, near-tip CTOA values, see Appendix B. The relation between COA- and $CTOA$-values was treated analytically in [10]. In the same paper, [10], a rule for estimating COA for various specimen sizes is proposed.

Eq.(14) and Eq.(17) in Appendix B, COD_{i} and COA can be transformed into the familiar J_{i}-and R-values.

To understand and to improve the fracture properties of two- or multi-phase materials, the determination of local fracture properties will be even more important. There, and in the field of microsystem technology, the new technique offers a vast variety of possible applications. A first example was presented in [42]: The crack growth resistance curves of the ferritic-austenitic steel A 905 shows a very strong influence of the crack-plane orientation. Via stereophotogrammetric studies it was possible to determine characteristic values for the fracture initiation toughness and to explain the different shapes of the resistance curves.

7. Final Discussion and Summary

In this study the total plastic strain energy for fracturing plain-sided CT specimens is separated into several components. The purpose of the separation is to find characteristic fracture energies which can be used for the characterization of the crack growth resistance of the material and for the prediction of the crack growth resistance for other specimen geometries and sizes. For the two materials investigated, the solution annealed maraging steel V 720 and the nitrogen alloyed ferritic-austenitic duplex steel A 905, the characteristic fracture energies are listed in Table V. J_{i} gives the commonly used fracture initiation toughness of the materials. R_{flat} describes the plastic strain energy for forming a unit area of the flat-fracture mid-section region. R_{flat} consists of a surface and a subsurface component. The surface component, R_{surf}, is the plastic strain energy to form the dimple structure of the fracture surface. R_{slant} describes the plastic strain energy for forming a unit area of the slant-fracture near side-surface regions. W_{lat} is the plastic strain energy for the lateral contraction and for the blunting process at the side-surfaces.

R_{flat} is found by analyzing the crack growth resistance curves of a plain-sided and a side-grooved specimen. The size of W_{lat} is estimated directly from the resistance curve of the plain-sided specimen. A comparison of the behavior of specimens with different thicknesses shows that W_{lat} remains constant as long as the two shear-lip regions remain separated by a flat-fracture region. The analysis of a thin specimen, where the two shear-lips merge into one slant-fracture surface, leads to the size of R_{slant}.

The crucial point for the extraction of the characteristic fracture properties is the analysis of total crack growth resistance curves (R_{tot}-Δa-curves) applying a single-specimen technique.

It is demonstrated that the characteristic fracture energies of the flat-fracture regime can be determined directly from the shape of the corresponding fracture surface regions on both specimen halves. J_{i} can be determined by mea-

suring the critical crack tip opening displacement, COD_{i}. The sub-surface component of $R_{\mathrm{flat}} = R_{\mathrm{surf}} + R_{\mathrm{sub}}$ can be evaluated from the crack opening angle, COA; the surface component is estimated via a model derived by Stüwe. A new system for the automatic analysis of fracture surfaces from stereophotograms generates tridimensional models of the depicted regions consisting of 10 000 to 20 000 points. From these models the necessary data for the evaluation of R_{surf} and R_{sub} can be extracted.

For the steel V 720 all the characteristic fracture energy components could be determined for four specimens with different thicknesses. The flat-fracture crack growth resistance of this material is not very large, $R_{\mathrm{flat}} = 280\,\mathrm{kJ/m^2}$. Only a very small part, $R_{\mathrm{surf}} = 20\,\mathrm{kJ/m^2}$, is necessary to form the micro-ductile fracture surface. The same R_{surf} is found at the begin and near the end of the transition region, and even in the fast-fracture region of a side-grooved specimen. The generation of a slant shear-lip fracture surface needs much more energy: $R_{\mathrm{slant}} = 1000\ \mathrm{kJ/m^2}$. A large part of the total crack growth resistance (22% to 61%) comes from lateral contraction and blunting at the side surfaces. It was found that the plastic work for the lateral contraction and the blunting at the side-surfaces, W_{lat}, remains constant as long as the specimen is thick enough, so that the shear-lip regions are separated by a flat-fracture region.

The steel A 905 has no shear-lips. Starting from a plateau-values of $R_{\mathrm{flat}} = 1000\ \mathrm{kJ/m^2}$, the flat-fracture crack growth resistance increases gradually towards the side-surface. R as a function of the distance from the side surface can be determined by stereophotogrammetric analyses. 22% of the total crack growth resistance comes from lateral contraction and blunting at the side surfaces.

Except for one specimen, the sum of local energy terms $\sum W_{\mathrm{pl,est}}$, determined according to the procedures described in this work, corresponds well with the experimentally measured value $W_{\mathrm{pl,tot}}$.

In this paper, two new techiques are applied to extract characteristic fracture energies from experiments. To solve the transferability problem similar experiments should be repeated, first, on CT- specimens with the same size but different ligament lengths, second, on CT-specimens with different sizes and, third, on different specimen types such as Center Cracked Tension (CCT-) or Double Edged Notched Tension (DENT-) specimens.

Acknowledgements

The authors thank Raj Thampuran for very helpful discussions during the writing of the paper. The authors acknowledge the financial support of this work by the *Austrian Fonds zur Förderung der wissenschaftlichen Forschung*

and by the *Österreichische Nationalbankfonds* (project numbers P11559-ÖTE / FWF 456 and P12278-MAT / FWF 482).

References

1. Turner C.E. (1990) in *Fracture Behavior and Design of Materials and Structures, Proc. ECF8* (edited by D. Firrao), EMAS, UK, Vol. II, pp. 933-949 and pp. 951-968.
2. Leevers P.S. and J. C. Radon (1982) *International Journal of Fracture* **19,** 311.
3. Hancock J.W., W. G. Reuter and D. M. Parks (1993) *ASTM STP* **1171,** 21.
4. O'Dowd N.P. and C. F. Shih,(1991) *Journal of Mechanics and Physics of Solids* **39,** 989 .
5. O'Dowd N.P. and C. F. Shih (1994) *ASTM STP* **1207,** 21.
6. Brocks W. and W. Schmitt (1995) *ASTM STP* **1244,** 209.
7. Kolednik O., G.X. Shan and F.D. Fischer (1997) *ASTM STP* **1296**, 126.
8. Kolednik O. (1993) *International Journal of Fracture* **63,** 263.
9. Braga L.and C. E. Turner (1993) *ASTM STP* **1171,** 158.
10. Turner C.E. and O. Kolednik (1997) *Fatigue and Fracture of Engineering Materials and Structures* **20,** 1507.
11. Turner C.E. and O. Kolednik (1994) *Fatigue and Fracture of Engineering Materials and Structures* **17** 1089.
12. Griffith A.A. (1920) *Philosophical Transactions of the Royal Society London* **A221,** 163.
13. Orowan E. (1945) *Transactions of the Institute of Engineers and Shipbuilders Scotland* **89,** 165.
14. Irwin G.R. (1949) in *American Society of Metals Seminar Fracture of Metals* pp. 147-166.
15. Hutchinson J.W. (1987) *Acta metallurgica* **35,** 1605.
16. Budiansky B., J. W. Hutchinson and A. G. Evans (1986) *Journal of Mechanics and Physics of Solids* **34,** 167.
17. Evans A.G. (1989) *ASTM STP* **907,** 267.
18. Atkins A.G. and Y. W. Mai (1986) *International Journal of Fracture* **30,** 203.
19. Gurney C. (1994) *Philosophical Magazine* **69,** 33.
20. Cotterell B. and J. K. Reddel (1977) *International Journal of Fracture* **13,** 267.
21. Wnuk M.P. and D. T. Read (1986) *International Journal of Fracture* **31,** 161.
22. Marchal Y. and E. Delannay (1996) *International Journal of Fracture* **80,** 295.
23. John S. and C. E. Turner (1991) in *Defect Assessment in Components; Fundamentals and Applications, ESIS/EGF Pub. 9* (edited by J. G. Blauel and K.-H. Schwalbe). MEP, London, pp. 299-318.
24. Shoji T. (1981) *Journal of Testing and Evaluation* **9,** 324.
25. Mao X.and T. Shoji (1993) *Journal of Materials Science* **28,** 927.
26. Stüwe H. P. (1990) *Engineering Fracture Mechanics* **13,** 231.
27. Stüwe H.P. (1981) in *Three-dimensional Constitutive Relations and Ductile Fracture* (edited by S. Nemat-Nasser). North-Holland, Amsterdam, pp. 213-221.
28. Kolednik O. and H. P. Stüwe (1982) *Zeitschrift für Metallkunde* **73,** 219.
29. Kolednik O. and H. P. Stüwe (1985) *Engineering Fracture Mechanics* **21,** 145.
30. Mecklenburg M.F., J. A. Joyce and P. Albrecht (1989) *ASTM STP* **995,** 594.
31. Scherer S., J. Stampfl, M. Gruber and O. Kolednik (1996) in *Micro Materials '95, 1. Tagung des DVM-Arbeitskreises Mikrosystemtechnik*(edited by B. Michel and T. Winkler). DVM, Berlin, pp. 671–676.

32. Stampfl J., S. Scherer, M. Gruber and O. Kolednik (1996) *Applied Physics A* **63,** 341.
33. Kolednik O. (1981) *Practical Metallography* **18,** 562.
34. Stampfl J., S. Scherer, H.P. Stüwe and O. Kolednik (1996) in *Mechanisms and Mechanics of Damage and Failure, Proc. of ECF 11* (edited by J. Petit). EMAS, UK, Vol.3, pp. 1271–1276.
35. Stampfl J., S. Scherer, M. Berchthaler, M. Gruber and O. Kolednik (1996) *International Journal of Fracture* **78,** 35.
36. ESIS P2-92 (1992) European Structural Integrity Society, Delft, The Netherlands.
37. ASTM E1152-87 (1993) Annual Book of ASTM Standards, Vol. 03.01.
38. Kolednik O. (1991) *Engineering Fracture Mechanics* **38,** 403.
39. Atkins A.G. (1995) *Fatigue and Fracture of Engineering Materials and Structures* **18** 1007.
40. Cotterell B. and A. G. Atkins (1996) *International Journal of Fracture* **81,** 357.
41. Stampfl J. (1996) PhD thesis, University of Mining and Metallurgy, Leoben.
42. Kolednik O., M. Albrecht, M. Berchthaler, H. Germ, R. Pippan, F. Riemelmoser, J. Stampfl and J. Wei (1996) *Acta Metallurgica et Materialia* **44,** 3307.
43. Krasowsky A.J. and V. A. Stepanenko (1979) *International Journal of Fracture* **15,** 203.
44. Bauer B. and A. Haller (1981) *Practical Metallography* **18,** 327.
45. Exner H.E. and M. Fripan (1985) *Journal of Microscopy* **139,** 161.
46. Kobayashi T. and J. H. Giovanola (1989) *Journal of Mechanics and Physics of Solids* **37,** 759.
47. Gruber M. and O. Kolednik (1992) in *International Archives of Photogrammetry and Remote Sensing, Proc. of ISPRS XVII* (edited by L. W. Fritz and J. R. Lucas). Vol. 29, Part B5, Comission V, pp. 305–310.
48. Bryant D. (1986) *Micron Microscopy Acta* **17,** 237.
49. Kobayashi T. and D. A. Shockey (1987) *Metallurgical Transactions* **18A,** 1941.
50. Gruber M.and W. Walcher (1994) in *International Archives of Photogrammetry and Remote Sensing, Proc. of ISPRS XVIII* . Vol. 30, Part 3/1, pp. 311–315.
51. Gerberich W. W. and E. Kurman (1985) *Scripta metallurgica* **19,** 295.
52. Kolednik O. and P. Kutleša, *Engineering Fracture Mechanics* **33,** 215.
53. Shan G. X. , O. Kolednik, F. D. Fischer and H. P. Stüwe (1993) *Engineering Fracture Mechanics* **45,** 99.
54. Dawicke D.S., R. S. Piascik and J. C. Newman, Jr. (1997) *ASTM STP* **1321,** 309.
55. Yan W.-Y. , G.X. Shan, O. Kolednik and F. D. Fischer (1998) *Key Engineering Materials* **145-149**, 179 .
56. Kolednik O. and H. P. Stüwe (1989) *International Journal of Fracture* **33,** R63 (1987).

Appendix

A. Some Remarks on the Reversibility of Fracture Energies

In a fracture experiment external energy which is provided by the testing machine, is transformed into elastic and plastic strain energy of the specimen and into surface energy. Most of the plastic strain energy is dissipated; only a small fraction, say 5%, is used to enhance the dislocation density in the plastic zone. This fraction of plastic energy could be recovered by annealing,

thus it is strictly speaking a reversible energy. However, we have to treat it as a non-reversible energy when considering the energy balance in a usual fracture experiment, unless the specimen is broken at such high temperatures that the material may recover.

When plastic flow occurs at the crack tip some portion of the elastic strain energy becomes non-reversible on unloading but remains as residual elastic energy, $W_{\mathrm{el,nr}}$, in the specimen. If the specimen bursted into thousands of tiny pieces during fracture this energy would be reversible and would act as an additional driving force for fracture.

B. The Relation between R and COA

The relation between the total crack growth resistance, R_{tot}, and the slope of the $J-\Delta a$ curve was presented already in [8, 38]. The derivation shall be repeated here briefly.

Differentiation of the J-evaluation formula, Eq.(7), with respect to the crack extension leads to

$$\frac{dJ}{d(\Delta a)} = \frac{\eta}{bB}\frac{dU}{d(\Delta a)} \tag{15}$$

For small Δa the error made by assuming that b and η remain constant is negligeable. After the plastic limit load has been reached the elastic strain energy remains approximately constant, and $dU = dW_{\mathrm{el}} + dW_{\mathrm{pl,tot}} \approx dW_{\mathrm{pl,tot}}$. Thus, Eq.(15) can be extended to

$$\frac{dJ}{d(\Delta a)} \approx \frac{\eta}{bB}\frac{dW_{\mathrm{pl,tot}}}{d(\Delta a)} = \frac{\eta}{b}R_{\mathrm{tot}}, \tag{16}$$

This relation holds for deeply notched bend and CT specimens.

To derive the relation between R_{tot} and the crack-opening angle we need the relationship between the J-integral and the crack opening displacement,

$$J = m\sigma_{\mathrm{y}}\, COD. \tag{17}$$

It shall be remarked that in Eq.(17) COD denotes the crack opening displacement at the position of the fatigue pre-crack (in contrary to the crack-tip opening displacement, $CTOD$, at the current crack tip position). The factor m depends primarily on the strain-hardening exponent of the material. For many materials, e.g. medium-strength steels, $m = 2$ is a quite good approximation, but usually not for low-strength materials with high strain-hardening exponent. It was demonstrated, [56], that Stüwe's estimate of the mean flow stress, Eq.(12), can be used to evaluate m from the tensile test data,

$$m = \frac{\sigma_{\mathrm{u}}}{\sigma_{\mathrm{y}}} \frac{\exp(n)}{(1+n)n^n}. \tag{18}$$

By differentiating Eq.(17) with respect to Δa and substituting Eq.(16) we get

$$COA = \frac{dCOD}{d\Delta a} \approx \frac{\eta}{m\sigma_{\mathrm{y}} b} R_{\mathrm{tot}}. \tag{19}$$

COA is the crack opening angle measured at the initial tip position (in contrary to the current tip value, $CTOA$).

Table I. Chemical composition of the maraging steel V720

C	Si	Mn	Mo	Ni	Co	Ti	Al
0.003	0.10	0.10	5.3	18.5	9.0	0.6	0.1

Table II. Chemical composition of the duplex steel A905

C	Si	Mn	P	S	Cr	Mo	Ni
0.017	0.37	5.15	0.021	0.002	25.63	2.04	4.04
V	W	Cu	Al	N			
0.06	0.49	0.10	0.009	0.34			

Table III. The separation of the total plastic strain energy for fracture, $W_{\mathrm{pl,tot}}$, into its components: the plastic energies for producing fracture initiation in the center, $W_{\mathrm{pl,i}}$, for forming the flat-fracture area, $W_{\mathrm{pl,flat}}$, for forming the slant-fracture area, $W_{\mathrm{pl,slant}}$, and for side-surface blunting and lateral contraction, $W_{\mathrm{pl,lat}}$. Except for the specimen A 905-25, the sum of the local energies, $\sum W_{\mathrm{pl,est}}$, corresponds well with the experimentally measured value $W_{\mathrm{pl,tot}}$

Specimen	Δa_{tot}	J_{i}	ΔA_{flat}	$\Delta A_{\mathrm{slant}}$	$W_{\mathrm{pl,i}}$	$W_{\mathrm{pl,flat}}$	$W_{\mathrm{pl,slant}}$	$W_{\mathrm{pl,lat}}$	$\sum W_{\mathrm{pl,est}}$	$W_{\mathrm{pl,tot}}$
	$[mm]$	$\left[kJ/m^2\right]$	$\left[mm^2\right]$	$\left[mm^2\right]$	$[J]$	$[J]$	$[J]$	$[J]$	$[J]$	$[J]$
V720-25	11.5	65	248	40	6.0	69	40	33	148	125
V720-16	7.4	60	102	15	3.0	29	15	29	76	68
V720-8	3.3	65	19.2	7.4	1.3	5.4	7.4	29	46	42
V720-4	3.0	65	10.8	5.2	0.6	3.0	5.2	17	26	28
V720-25sg	0.6	70	12.0	0	1.8	3.4	0	0	5.2	4.6
A905-25	3.5	200	88	0	33	88	0	45	146	207
A90-25sg	2.7	190	53	0	27	53	0	0	80	70

Table IV. The plastic strain energy to form a unit area of the micro-ductile flat-fracture surface for a plain-sided and a side-grooved specimen.

Specimen	Distance from fatigue crack	R_{surf}
	mm	kJ/m^2
V720-25	0.1	23
	0.1	16
	2.0	19
V720-sg	3.0	20

Table V. The characteristic fracture energies determined on deeply notched CT specimens.

Material	J_{i}	R_{surf}	R_{flat}	R_{slant}	W_{lat}
	$[kJ/m^2]$	$[kJ/m^2]$	$[kJ/m^2]$	$[kJ/m^2]$	$[J]$
Steel V 720	65	20	280	1000	30
Steel A 905	190	?	1000	–	45

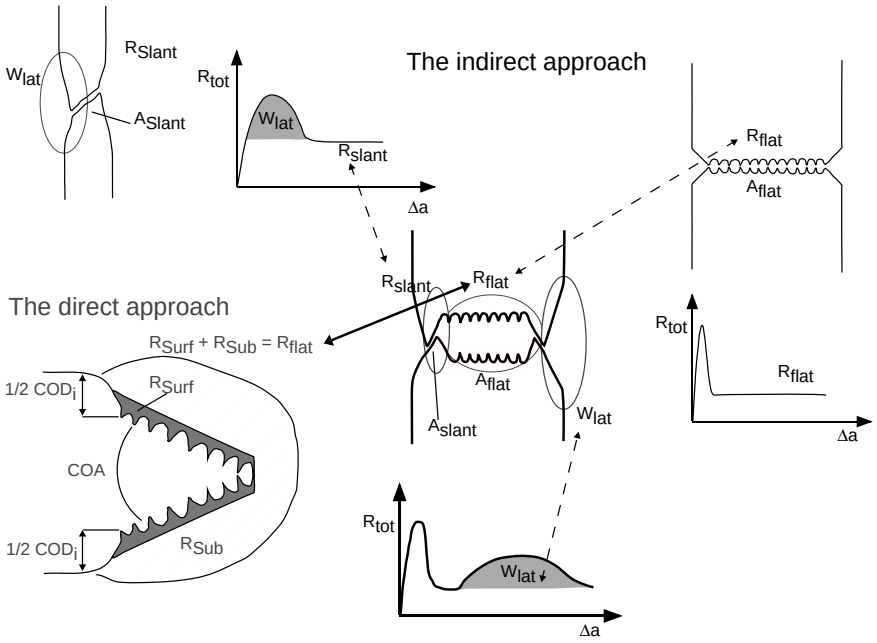

Figure 1. A schematic view of the indirect and the direct approach to separate the fracture energies.

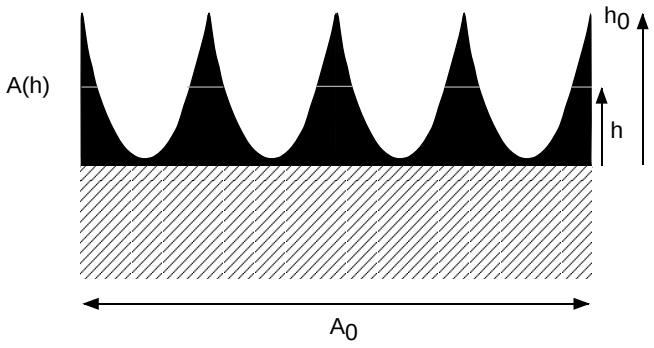

Figure 2. A schematic crossection of a micro-ductile fracture surface to Stüwes model for the estimation of R_{surf}

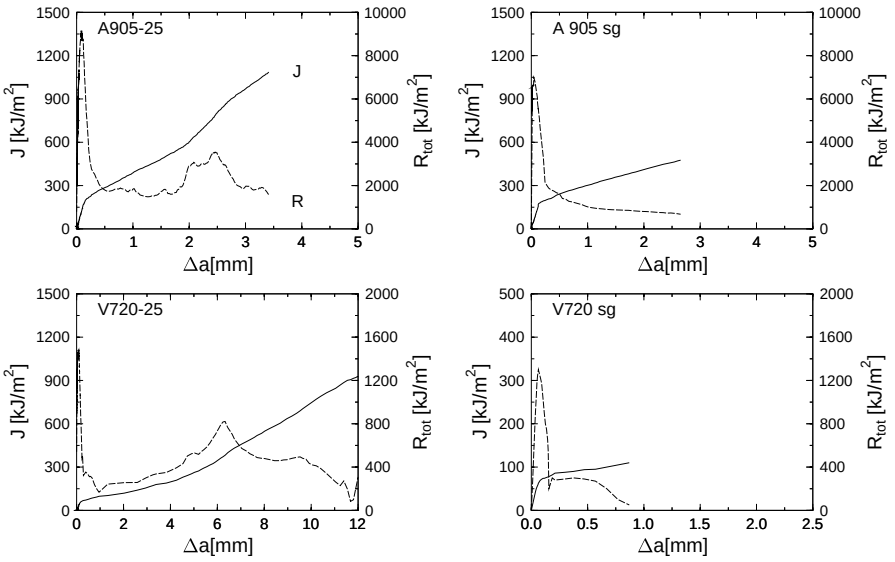

Figure 3. J-integral, J (solid line), and total crack growth resistance, $R_{\rm tot}$ (dashed line), with respect to the crack extension , Δa, for 25 mm thick specimen with and without side-grooves. Note the different scales.

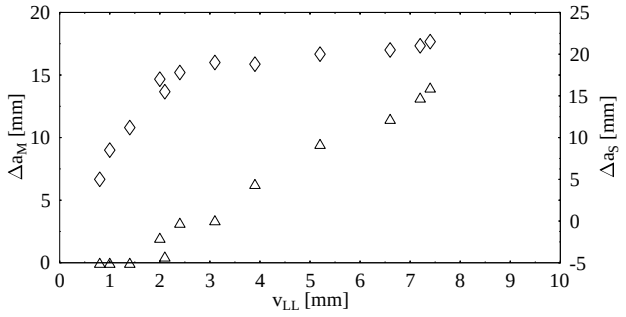

Figure 4. Local crack in the mid-section region $\Delta a_{\rm M}$ ($\Diamond$), and at the side-surfaces, $\Delta a_{\rm S}$ ($\triangle$), with respect to the load line displacement, $v_{\rm LL}$, for plain sided specimens of the steel V 720.

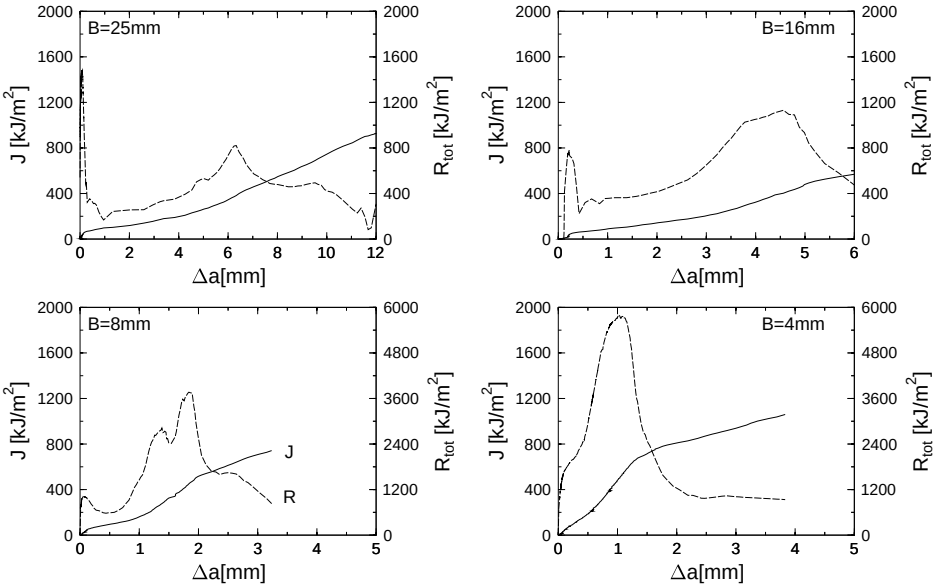

Figure 5. J-integral, J (solid line), and total crack growth resistance, $R_{\rm tot}$ (dashed line), with respect to the crack extension , Δa, for plain-sided specimens of different thickness. Steel V 720. Note the different scales.

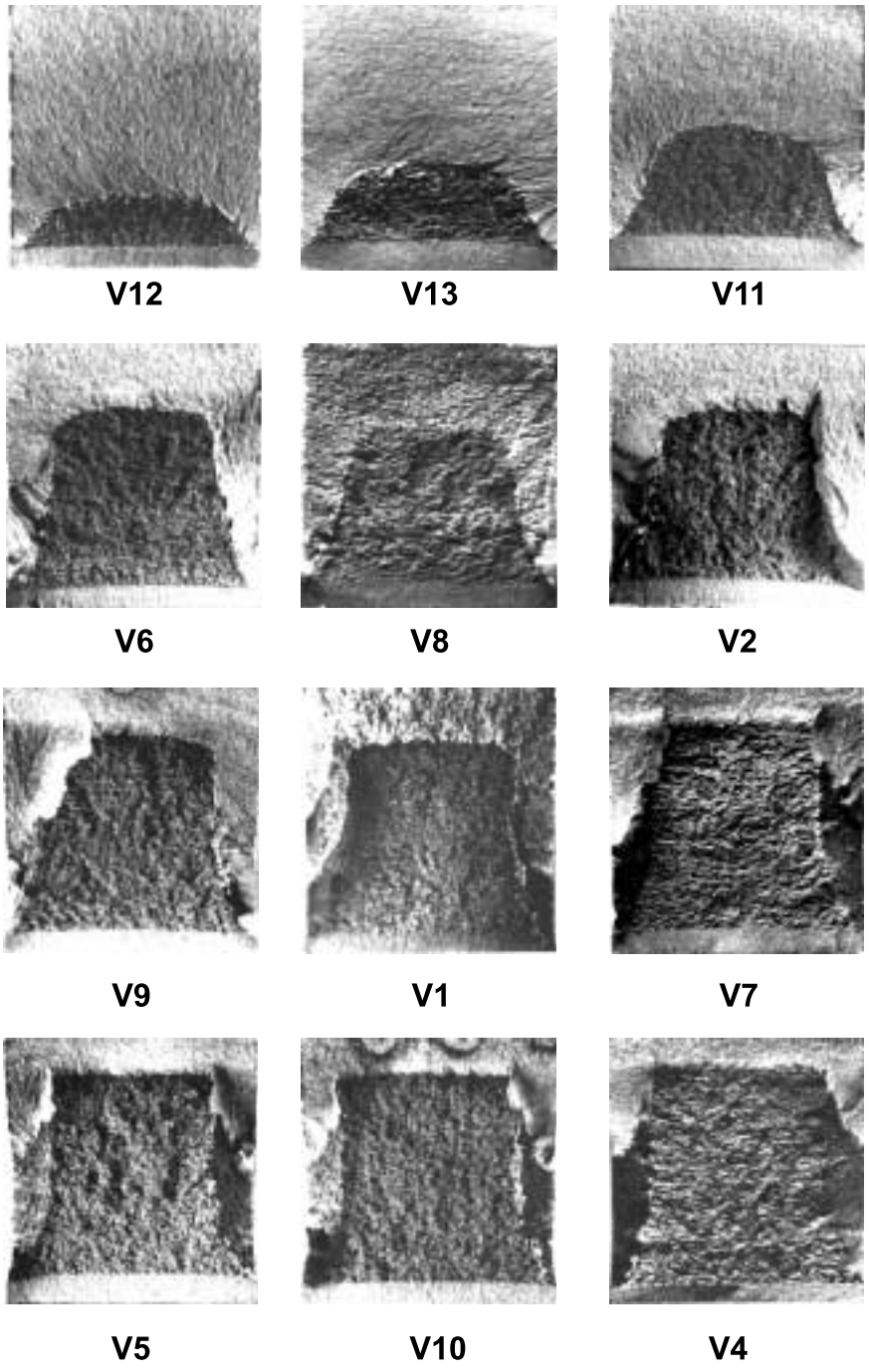

Figure 6. Heat-tinted fracture surfaces of the V720-specimens from the multi-specimen test. The specimen thickness is 25 mm

Figure 7. Fracture surface of a plain-sided specimen made of steel A 905. Note the large lateral contraction and the increased width of the stretched zone near the side-surfaces.

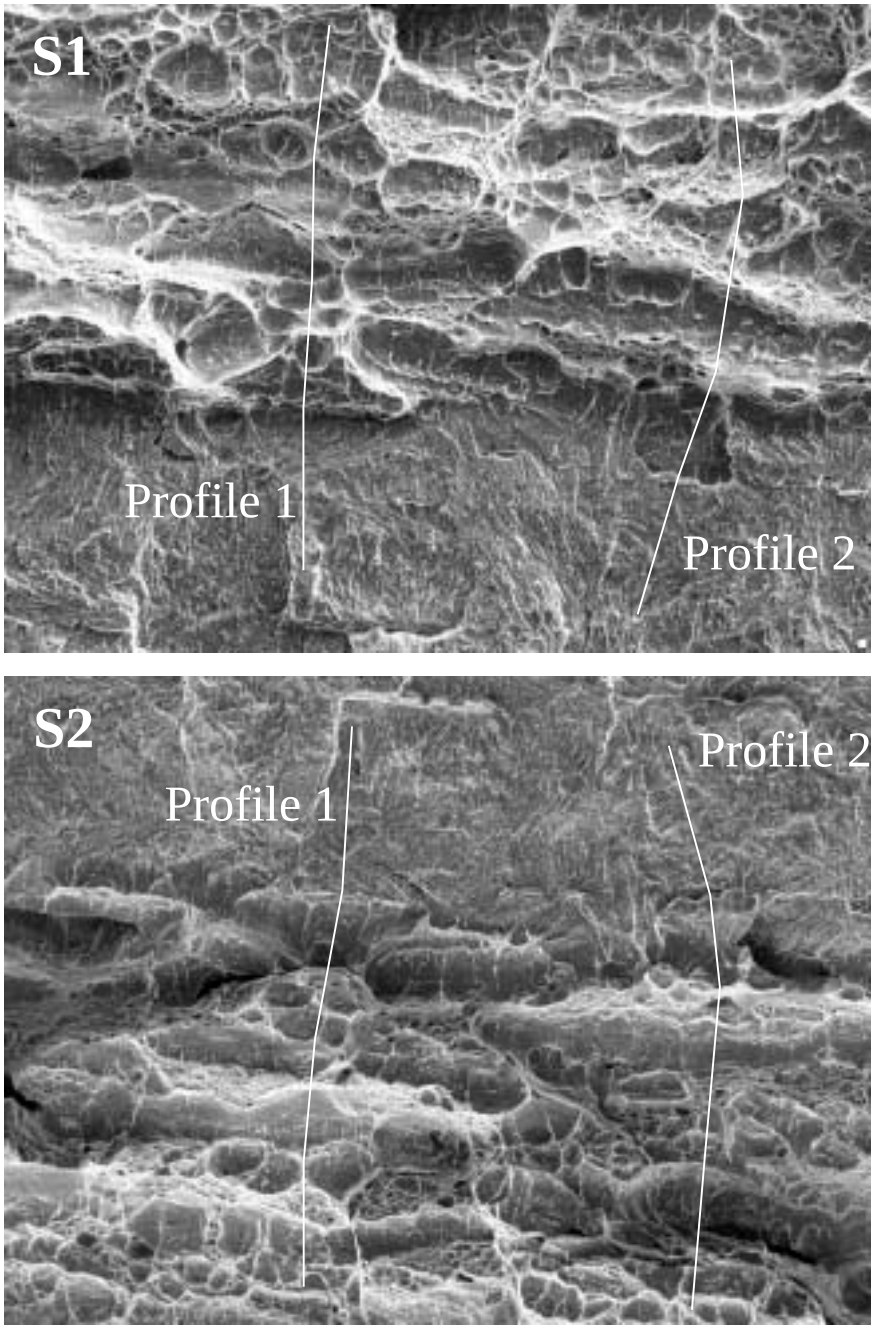

Figure 8. Corresponding fracture surfaces of the maraging steel V 720. The digital elevation models (DEMs) of the fracture surfaces are shown in Fig. 9, the crack profiles are presented in Fig. 10.

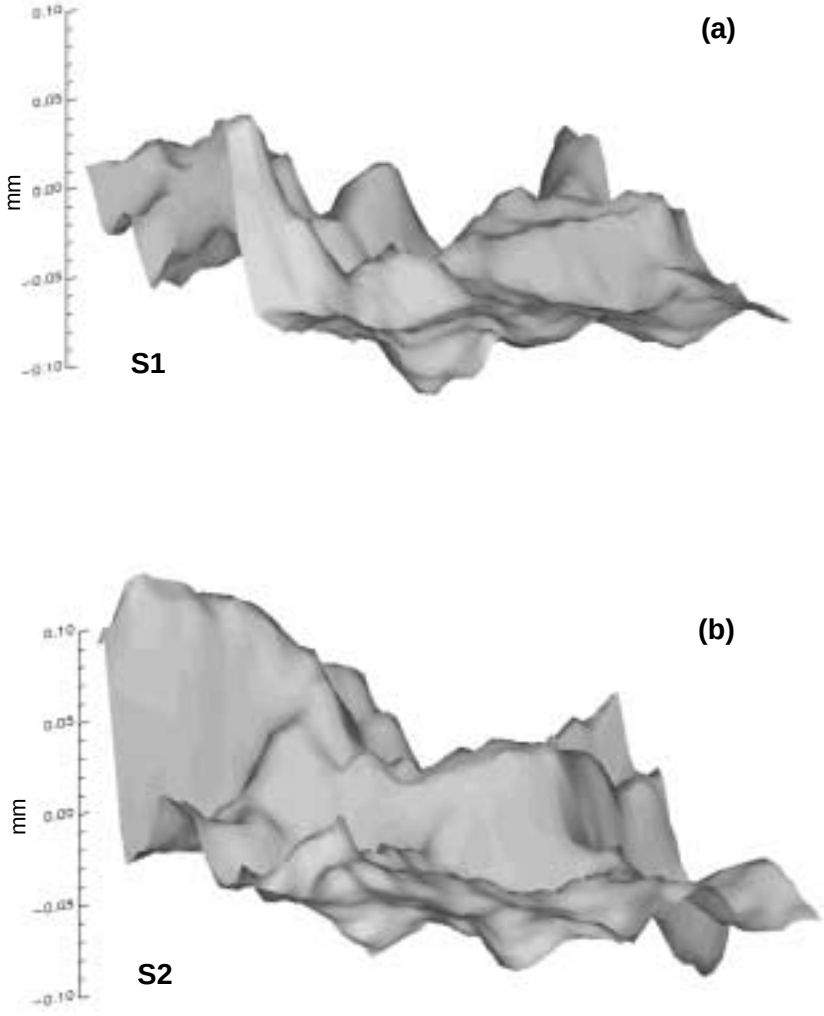

Figure 9. DEMs of the fracture surfaces in Fig. 8. Both specimen halves, side 1 (a) and side 2 (b), are shown.

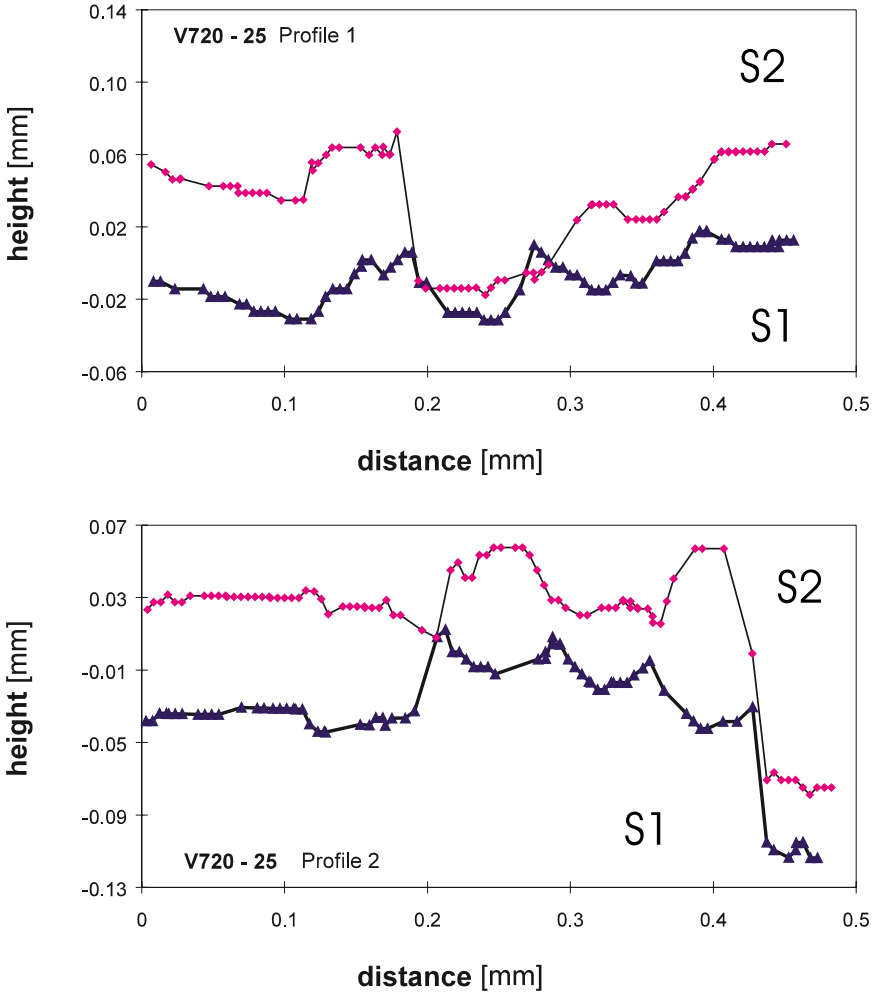

Figure 10. Crack profiles from the fracture surfaces in Fig. 8

List of Tables

I	Chemical composition of the maraging steel V720	23
II	Chemical composition of the duplex steel A905	23
III	The separation of the total plastic strain energy for fracture, $W_{\mathrm{pl,tot}}$, into its components: the plastic energies for producing fracture initiation in the center, $W_{\mathrm{pl,i}}$, for forming the flat-fracture area, $W_{\mathrm{pl,flat}}$, for forming the slant-fracture area, $W_{\mathrm{pl,slant}}$, and for side-surface blunting and lateral contraction, $W_{\mathrm{pl,lat}}$. Except for the specimen A 905-25, the sum of the local energies, $\sum W_{\mathrm{pl,est}}$, corresponds well with the experimentally measured value $W_{\mathrm{pl,tot}}$	24
IV	The plastic strain energy to form a unit area of the microductile flat-fracture surface for a plain-sided and a side-grooved specimen.	25
V	The characteristic fracture energies determined on deeply notched CT specimens.	25

List of Figures

1 A schematic view of the indirect and the direct approach to separate the fracture energies. 26

2 A schematic crossection of a micro-ductile fracture surface to Stüwes model for the estimation of R_{surf} 26

3 J-integral, J (solid line), and total crack growth resistance, R_{tot} (dashed line), with respect to the crack extension , Δa, for 25 mm thick specimen with and without side-grooves. Note the different scales. 27

4 Local crack in the mid-section region Δa_{M} ($\Diamond$), and at the side-surfaces, Δa_{S} ($\triangle$), with respect to the load line displacement, v_{LL}, for plain sided specimens of the steel V 720. 27

5 J-integral, J (solid line), and total crack growth resistance, R_{tot} (dashed line), with respect to the crack extension , Δa, for plain-sided specimens of different thickness. Steel V 720. Note the different scales. 28

6 Heat-tinted fracture surfaces of the V720-specimens from the multi-specimen test. The specimen thickness is 25 mm 29

7 Fracture surface of a plain-sided specimen made of steel A 905. Note the large lateral contraction and the increased width of the stretched zone near the side-surfaces. 30

8 Corresponding fracture surfaces of the maraging steel V 720. The digital elevation models (DEMs) of the fracture surfaces are shown in Fig. 9, the crack profiles are presented in Fig. 10. 31

9 DEMs of the fracture surfaces in Fig. 8. Both specimen halves, side 1 (a) and side 2 (b), are shown. 32

10 Crack profiles from the fracture surfaces in Fig. 8 33